International Journal of Power and Energy Systems, Vol. 44, No. 10, 2024
An Open Access Paper

NEURAL NETWORK BASED DATA QUALITY MONITORING AND REAL-TIME ANALYSIS METHOD FOR ENERGY STORAGE POWER PLANTS

Xiuquan Li,* Mingwan Zhuang,* Weirong Yang,* Xiaohong Zhu,* and Qiyuexin Wang*

Abstract

The rapid expansion of China's urban railway transport sector has heightened the need to minimise the substantial train energy consumption. Ground-mounted supercapacitor (SC) energy storage plants have proven to be effective in reclaiming regenerative braking energy and are hence, valuable in reducing train energy usage. To enhance efficiency, the present study refines the energy management approach utilising the conventional voltage–current double-loop control strategy while considering both the operational state of the train and the energy storage power station demand. To conduct simulation experiments, an exclusively designed platform for urban rail transportation power supply systems is employed, with the Batong Line of the local metro used as the sample. The key novelty of this investigation is a regenerative energy (RE) forecasting model that employs a neural network. This model takes into account both the current location and power of the train to make precise predictions about the RE needs of the energy storage facility. The study demonstrated that the improved strategy resulted in a decrease in output energy usage by 0.2 kWh within the substation and a reduction in energy expenditure on the braking resistor by 0.178 kWh, making it highly beneficial in terms of energy conservation when compared to the fixed-threshold strategy. Hence, the study provides a useful technical reference for energy-saving initiatives in urban rail transportation and has practical applicability.

Key Words

Neural network, energy storage power plant, urban rail transit, regenerative energy, dynamic thresholds

* Qujing Power Supply Bureau, Yunnan Power Grid Co. Ltd., Qujing 655000, China; e-mail: lxq532822995@163.com
Corresponding author: Xiuquan Li

(DOI: 10.2316/J.2024.203-0534)

1. Introduction

Due to China's rapidly developing economy and urbanisation, an influx of people are migrating to cities. This has resulted in an escalation in traffic congestion and environmental issues [1], [2]. Consequently, urban rail transit (URT) has emerged as a vital solution for large and medium-sized cities, due to its high capacity, safety, efficiency, and low pollution levels [3], [4]. However, the majority of regenerative energy (RE) produced during braking is transformed into heat, squandering valuable energy and leading to increased maintenance expenses. In spite of the fact that the current ground-mounted supercapacitor (SC) energy storage system (ESS) can salvage some of the energy, its management approach is still inadequate [5], [6]. To achieve the goal, present a management strategy is presented for dynamic thresholds (DT) that incorporates a back propagation neural network (BPNN) in the context of an energy storage power plant (ESPP). The use of BPNN allows us to accurately forecast the charging demand of the ESPP. This prediction data is then used to dynamically adjust the ESPP thresholds, ensuring an even distribution of energy across power stations and optimising the use of renewable energy. The study comprises the following parts: Part one provides an overview of the research results and limitations of SC and ESPP systems at both domestic and international levels. In Part two, a DT management strategy integrating BPNN in the context of ESPP is devised. Part three analyses and simulates the anticipated RE and DT management strategy. Part four presents a summary of the experimental outcomes, highlights the study's drawbacks, and proposes future research directions.

2. Related Works

SC energy storage is extensively employed in URT. Several energy management strategies have been suggested for diverse areas to optimise the multiple aspects and ensure

the effective operation of ESPP devices, tackle operational problems and boost the performance of SCs [7], [8]. To effectively integrate a SC ESPP into a wind energy multi-area power system, Nisa and Mufti proposed a discrete mode control strategy. The study designed the main control loop of the SCS power plant to simulate its response. This strategy not only ensures that the SCS power plant closely follows the commands of the main controller but also reduces frequency and power deviations. Finally, a simulation platform was created in MATLAB/Simulink to verify the effectiveness of the method [9]. Mali and Tripathi explored the use of SCs as electrical energy storage components. The study investigated the performance of SCs in light electric vehicles using WLTC driving profiles through MATLAB/Simulink. The results showed that the temperature had a large effect on the SC. At the same time, the SC can adapt to the low discharge current demand of the battery, reduce heat generation and outperform lithium-ion batteries [10]. Shadabi and Kamwa proposed an improved sag controller based on VICRC. This controller quickly suppresses the DC link voltage deviation. SC is responsible for compensating the high frequency demand and BESS compensates the low frequency demand. This helps in SOC recovery for SC energy storage. The wind farm and AC/DC grid converter models were simulated on the IEEE test system of Simulink/SPS and the results were extensively analysed to verify the benefits of the proposed structure [11].

Currently, artificial neural networks are widely used in power systems. Bento MEC believes that the load margin of the power system is an important indicator of the operation centre of the power system, and therefore proposes a physically guided neural network to calculate the load margin of the power system. This network regularises through auxiliary processes, and then reconstructs the power flow equation at the stability threshold that defines the load margin. The results show that the performance of this network is significantly better than traditional neural networks [12]. To characterise the uncertainty of wind power, Liao *et al.* proposed a new method for ultra short term interval prediction of wind power based on graph neural networks and improved Bootstrap technology. The simulation results show that this method can capture spatiotemporal correlations from the graph, and the prediction results are significantly better than the popular baselines on two real datasets [13]. Kiannejad *et al.* proposed an adaptive bidding strategy program based on a two-stage artificial neural network. The program mainly achieves this by revealing, modelling, and predicting the clustering behaviour of competitors in the hourly electricity market. The results show that the proposed method is sufficient to consider transmission constraints and has excellent performance. Kiannejad *et al.* believe that providing an effective optimal bidding strategy is crucial for load aggregators to increase their profits. Therefore, a two-stage artificial neural network-based adaptive bidding strategy program is proposed to reveal, model, and predict the clustering behaviour of competitors in the hourly electricity market. The results show that the strategy proposed by the research institute has significant effectiveness [14]. Li *et al.* found that the instability of the short-term voltage after the disturbance seriously affected the performance of the classifier. Therefore, a short-term voltage stability assessment method for transformer-based data-driven power system is proposed. The results show that the proposed method exhibits robust performance in noisy environments under up to 100:1 class imbalance, with consistent efficiency even with increased renewable energy permeability [15].

Mohammadamin *et al.* proposed an innovative approach that combines machine learning techniques, energy forms and their applications in different fields to classify and identify machine learning models. It also proposed that hybrid machine learning models are outstanding in improving the accuracy, robustness and generalisation of models in energy systems. This hybrid approach is particularly suitable for predictive models of renewable energy systems, such as solar and wind energy, and contributes significantly to improving energy efficiency and supporting energy governance and sustainable development [16]. Mosavi *et al.* believe that the core of ensuring smart grid security lies in the development and implementation of effective cyber defense strategies. A zero-sum Nash equilibrium strategy based on deep Q learning is proposed. The strategy has been demonstrated on Wood and Wollenberg six bus systems, as well as the larger IEEE 30 bus system, showing its advantages over traditional Q learning methods. In addition, comparisons with other reinforcement learning strategies also confirm the broad applicability of deep Q learning frameworks in securing modern power grids [17]. Moradi *et al.* proposed to develop a reinforcement learning method designed to satisfy the linear temporal logic preference description. The method transforms the preference satisfaction measure into a mixed integer programming problem, combines probabilistic programming techniques, and integrates it into the resource allocation problem to derive the optimal strategy through reinforcement learning. Due to the time-varying nature of the problem, each time step requires the solution of mixed integer programming. Validation on a standard W&W six bus grid model shows that the machine learning framework can protect systems against attacks in resource-constrained situations. Although the current approach is computationally demanding, it lays the foundation for the development of efficient machine learning frameworks for large-scale networks [18].

SC energy storage has found widespread use and research in various fields; however, insufficient attention has been given to its adoption in the field of ESPP for URTs. The current energy management strategy is inadequate as the simulation model is excessively idealised and fails to account for the intricacy of the DC traction power supply network and the actual power of the SC. Therefore, a novel energy management approach is proposed utilising BPNN energy prediction that considers the voltage fluctuation of the substation. Our objective is to minimise output energy and reduce the consumption of braking resistor energy.

3. BPNN-Based Prediction of RE With DT Management Strategy

The study introduces a prediction and DT management strategy for RE based on BPNN. Firstly, the calculation method of how SC absorbs RE in ESPP is detailed. Then, the impact of charging threshold on the ESS is analysed through a simulation model. This research aims to reduce the output of ESPP.

3.1 BPNN-Based RE Prediction Method

To improve the comprehensibility of the model, the study has standardised the symbols used in the model, and the detailed symbols and their corresponding meanings are listed in Table 1. This step is designed to ensure the conceptual clarity and the accuracy of the calculations.

To ensure consistency and ease of reference for all relevant terms, the study developed a glossary detailing the individual professional terms and their definitions, as shown in Table 2.

In the URT system, although the current train position and power can be used to calculate the RE for ESPP, it is challenging to directly predict the total energy required due to the uncertainty of the train status. This uncertainty arises from operational contingencies and variations in departure intervals. To address this challenge, the study employs the nonlinear mapping capability of BPNN to predict the residual RE difference for ESPP. Using the URT power supply simulation data, the BPNN is trained to build an energy prediction model. The RE generated by train braking, in addition to being used by the traction vehicle and auxiliary power supply system, the ESPP absorbs the remaining energy if the energy storage capacity is sufficient [19], [20]. The study considers the RE to be absorbed during SC charging through a DC power supply model and simulates it using data from the Metro Octopus line, as shown in Fig. 1.

When the energy recovered by the train braking can be supplied to the nearby traction vehicle in addition to the auxiliary power system, it can also be stored by the energy storage station, provided that the energy storage capacity of these facilities is sufficient. This study defines the residual RE, that is, the energy after the utilisation of the auxiliary power supply system, the consumption of tractors, various energy consumption and the absorption of other energy storage facilities is deducted from the braking energy recovered by the train. To estimate the remaining RE absorbed by the SCs before a full charge, a DC power supply model is developed with an energy storage station and based on eight-channel line data. During charge and discharge, the voltage value of the power supply corresponds to the threshold of charge and discharge, respectively. To simplify the study, let there be only one train between Orchard and Pearland stations, whose distance to ESPP (ESS1) at Orchard station is x and its power is P_r. For the specific model, see Fig. 2.

As shown in Fig. 2, the corrected nodal voltage equation is written as shown in (1).

$$\begin{bmatrix} y_{\text{eq1}}+y_{11}+y_4 & -y_4 & 0 & -y_{11} & 1\ 0\ 0 \\ -y_4 & y_{\text{eq2}}+y_{2+3+4+12} & -y_2-y_3 & -y_{12} & 0\ 1\ 0 \\ 0 & -y_2-y_3 & y_{\text{eq3}}+y_2+y_3 & 0 & 0\ 0\ 1 \\ -y_{11} & -y_{12} & 0 & y_{11}+y_{12} & 0\ 0\ 0 \\ 1 & 0 & 0 & 0 & 0\ 0\ 0 \\ 0 & 1 & 0 & 0 & 0\ 0\ 0 \\ 0 & 0 & 1 & 0 & 0\ 0\ 0 \end{bmatrix} \begin{bmatrix} U_1 \\ U_2 \\ U_3 \\ U_T \\ U_{\text{ESS1}} \\ U_{\text{ESS2}} \\ U_{\text{ESS3}} \end{bmatrix} \tag{1}$$

In (1), y_{eq} and y_i represent specific voltage and current variables. The value of the guide y_{11} and y_{12} is related to the position. The subject circuit current is shown in (3).

$$I_1 = y_{\text{eq1}}U_0; I_2 = y_{\text{eq2}}U_0; I_3 = y_{\text{eq3}}U_0; \tag{2}$$

$$\begin{cases} \frac{P_T}{U_T}; U_T \le U_{\text{br}} \\ \frac{P_T}{U_T} - I_{\text{bra}}; U_T > U_{\text{br}} \end{cases} \tag{3}$$

In (3), U_{br} represents the braking resistor starting voltage; I_{br} represents the current on the braking resistor. The values of line conductance y_{11} and y_{12} are related to the position, assuming that the distance from the up train to the orchard station is x, the distance is $l-x$, as shown in (5).

$$y_{11} = \frac{1}{\text{rx}} \tag{4}$$

$$y_{12} = \frac{1}{r(l-x)} \tag{5}$$

In (5), l denotes the distance between two substations; r denotes the unit impedance. Based on the above analysis, the network quantities can be solved by knowing the train position and power while ignoring the no-load voltage fluctuation of the substations. After determining x and P_r, the current model is stable and the system voltage and current can be resolved and the RE of the$i$th SC ESPP at t_1 is known, as shown in (6).

$$E_{SC-in.i} = \int_{t_0}^{t_1} U_{\text{ESS},i} \cdot I_{\text{ESS},i} \cdot \eta_b \text{dt}, i = 1,2,3 \tag{6}$$

In (6), η_b denotes the conversion efficiency of the ESPP bi-directional DC/DC; the voltage $U_{\text{ESS},i}$ at both ends denotes the charging threshold equal to its counterpart; t_0 denotes the start moment; and t_1 denotes the current charging moment. In the URT system, the charging and discharging of SCs are not alternated in an ideal sequence. The ESPP may be in multiple charging or discharging states consecutively due to the energy flow between trains, between trains and substations, and between trains and

Table 1
Detailed Symbols and Their Corresponding Meanings

Variable	Explain
x	There is only one train between Guoyuan and Liyuan Station, the distance between it and Guoyuan Station (ESS 1)
P_r	Power
y_{eq}, y_i	Column write correction node voltage equation (Specific voltage and current variables)
y_{11}, y_{12}	The value of the line signer is related to the position
U_{br}	Represents the braking resistor starting voltage
I_{br}	Denotes the current on the braking resistor
η_b	Denotes the conversion efficiency of the ESPP bi-directional DC/DC
$U_{\mathrm{ESS},i}$	At both ends denotes the charging threshold equal to its counterpart
t_0, t_1	Denotes the start moment and the current charging moment
E_{SC-in}	Denotes the RE that has been absorbed from the beginning of the charging process to the current moment
$E_{SC-in\,\max}$	Denotes required to absorb the total regenerative energy
E_p	Residual regeneration energy difference
X_1, X_n	Network input
Y_1, Y_m	Predicted output
w_{ij}, w_{jk}	Weight
$w_{\mathrm{ij}}(t+1)$	Update of weights
$B_{\mathrm{ij}}(t+1)$	Updates of thresholds
m, n	Number of output-layer nodes
a	Denotes the number of values between 0 and 10
N_s	Denotes the number of samples used for training
x_i	Denotes the ith dimension data of the input variable
$x_{\max}$, $x_{\min}$	Denotes the maximum and minimum values in the input variable
P_{ESS}	Denotes the charging power of the ESPP
P_{br}	Indicates that it is the power on the braking resistor
P_t	Denotes the traction power of the train
P_{ss}	Denotes the total output power of the three substations
U_{char}	Denotes the voltage outer loop charging threshold
u_{SC}	Denotes the supercapacitor module terminal voltage
U_{dis}	Denotes the discharging threshold
ΔU_{dis}, ΔU_{char}, k	Denotes the three to-be-determined parameters
C, $U_{\max}$	Denote the container and maximal point voltages of the supercapacitor storage device, respectively
E_r	Denotes the residual energy storage capacity

the ESPP. The study defines a consecutive charging state as a charging process, *i.e.*, a charging process between two discharges, as shown in Fig. 3. The charging process is assumed to start at t_0 and end at t_2, with t_1 being any moment in the charging.

In Fig. 3, E_{SC-in} denotes the RE that has been absorbed from the beginning of the charging process to the current moment; $E_{SC-in\,\max}$ denotes the total RE that needs to be absorbed. Define the remaining RE difference E_p as the difference between the two, as

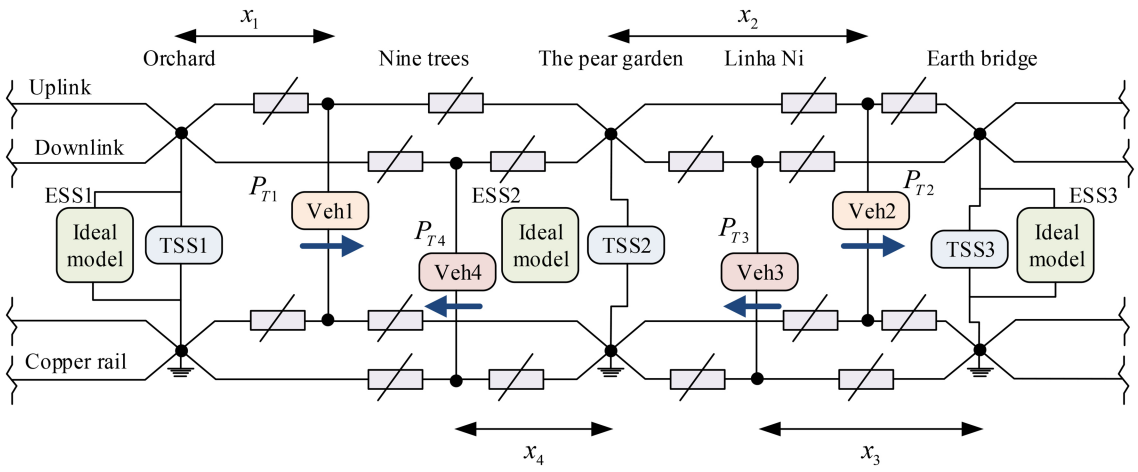

Figure 1. Ideal model of urban rail DC power supply system.

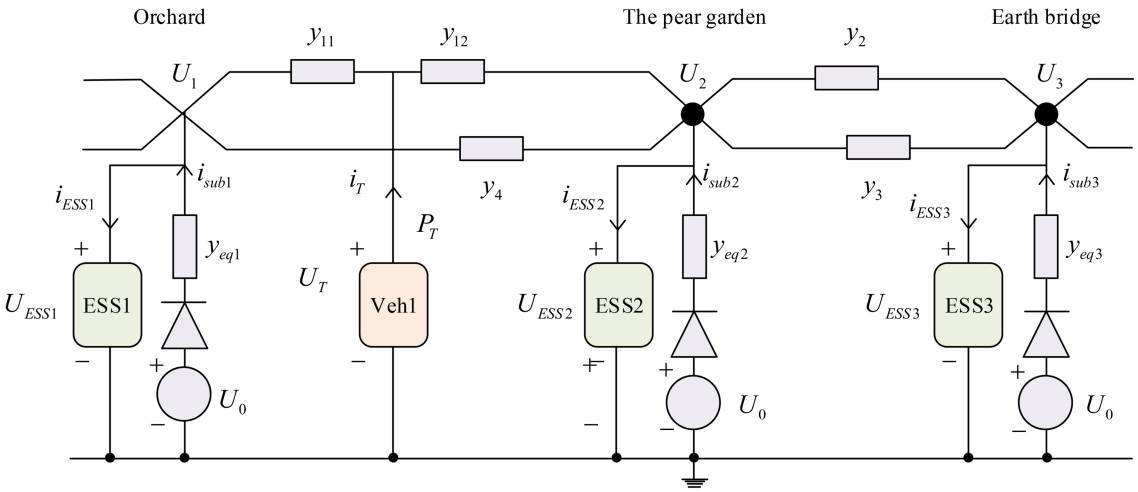

Figure 2. Urban rail traction power supply system model diagram.

Table 2
Technical Terms and Their Definitions

ESS	Energy storage system
BPNN	Back propagation neural network
L-M	Levenberg-Marquardt algorithm
FTP	Fixed threshold policy
ICS	Improved control strategy

shown in (7).

$$E_p = E_{SC-in\max} - E_{SC-in} \tag{7}$$

3.2 RE Prediction Model Construction Based on BPNN

BPNN is a feed forward network based on error back propagation. It can be trained with samples to obtain the mapping relationship between inputs and outputs, and is characterised by its simplicity and applicability, making it the most commonly used artificial neural network model.

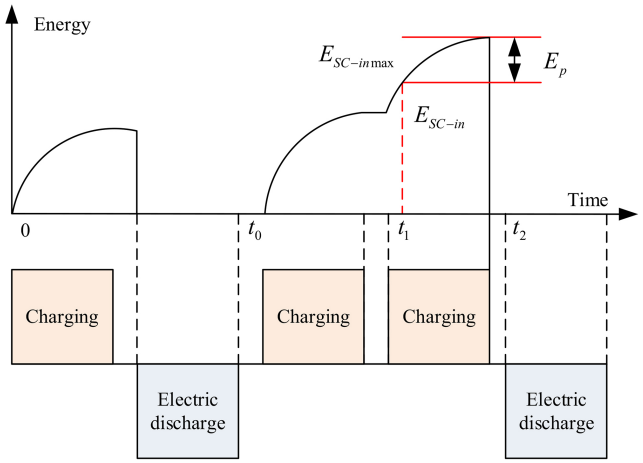

Figure 3. Schematic diagram of charging and discharging a supercapacitor.

The topology of this model contains three or more layers covering the input layer, one or more hidden layers and the output layer [21], [22], as shown in Fig. 4. Among them, X_1 to X_n are the network inputs, Y_1 to Y_m are the predicted

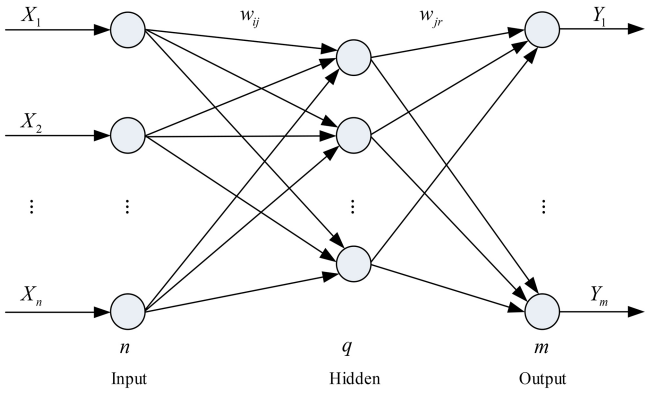

Figure 4. BP neural network topology structure diagram.

outputs, w_{ij} and w_{jk} represent the weights, and the hidden layer nodes often use Sigmoid excitation functions.

The BP algorithm mainly regulates the weights and thresholds to approximate the nonlinear problem. The learning process is divided into two steps: forward propagation and error back propagation. In forward propagation, the input signal is transmitted to the output layer through the implicit layer, and the weights and thresholds are unchanged. If the output error is large, it enters the backward propagation: from the output layer to the input layer, the error is shared by node, and the weights and thresholds are adjusted according to the error; nodes with large errors are adjusted more. The weights are updated as shown in (8).

$$\begin{aligned} w_{\mathrm{ij}}(t+1) &= -\eta\frac{\partial E}{\partial w_{\mathrm{ij}}} + w_{\mathrm{ij}}(t), w_{\mathrm{jk}}(t+1) \\ &= -\eta\frac{\partial E}{\partial w_{\mathrm{jk}}} + w_{\mathrm{jk}}(t) \end{aligned} \tag{8}$$

In (8), E denotes the prediction error. The threshold is updated as shown in (9).

$$\begin{aligned} B_{\mathrm{ij}}(t+1) &= -\eta\frac{\partial E}{\partial B_{\mathrm{ij}}} + B_{\mathrm{ij}}(t), B_{\mathrm{jk}}(t+1) \\ &= -\eta\frac{\partial E}{\partial B_{\mathrm{jk}}} + B_{\mathrm{jk}}(t) \end{aligned} \tag{9}$$

With the known power and speed of the train, this research was able to solve for each information of the line and calculate the RE E_{SC-in} absorbed by the SC. Offline simulation provided the maximum RE $E_{SC-in\,\max}$ during charging, yielding the residual RE difference E_p. A neural network was trained using the offline data to form the RE prediction model. In practice, a prediction model is used to estimate the difference between E_{SC-in} and the current E_{SC-in} to obtain the current E_p. To simplify the online computation and reduce the measurement error, the study chooses the E_p obtained offline as the expected value of the neural network. The BPNN contains an input layer, an output layer, and an implicit layer. The hidden layer can be single or multi-layer, and multi-layer provides higher prediction accuracy but longer training time. Based on the needs of this research, a single implicit layer structure is chosen. The number of input and output nodes is determined by the actual problem, here the model has eight input nodes (position and power of four trains) and one output node (remaining RE difference E_p). The choice of the number of nodes in the hidden layer is critical, too many may lead to "overfitting", while too few may reduce the accuracy of the model, as shown in (12).

$$l = \sqrt{(m+n)} + a \tag{10}$$

$$l = \log_2^n \tag{11}$$

$$l = \frac{m+n}{2} + \sqrt{N_s} \tag{12}$$

In (8), m denotes the number of output layer nodes; n denotes the number of input layer nodes; l denotes the number of implied layer nodes; a denotes a number between 0 and 10; and N_s denotes the number of samples for training. Since the nodes of input and output in this study are 8 and 1, respectively, and the number of samples is 1,000, the number of implied layer nodes is 104. In simulating the three-station, four-car urban rail system, the SC ESPP adopts an ideal model using the Octopus line parameters. The offline data is obtained through the urban rail traction power supply simulation system. Through simulation, the maximum RE $E_{SC-in\,\max}$ for each charging process is calculated and subtracted from the current E_{SC-in} to obtain E_p. To improve training efficiency and prediction accuracy, the data needs to be normalised so that its value ranges between [-1,1] as shown in (13). Normalisation helps to improve the learning speed and increase the accuracy of the prediction results.

$$y = \frac{2(x_i - x_{\min})}{x_{\max} - x_{\min}} - 1 \tag{13}$$

In (13), x_i denotes the ith dimension data of the input variable; $x_{\max}$ denotes the maximum value in the input variable; $x_{\min}$ denotes the minimum value in the input variable; and y denotes the result of x_i after normalisation. Continuously iterating until the result meets the requirements leads to the BPNN module, as shown in Fig. 5.

3.3 DT Management Strategy Based on BPNN Energy Prediction

The charging threshold of the ESPP has an impact on the tidal current distribution of the metropolitan rail power system. In most of the tidal current calculations, which are based on the ideal voltage source model, the power and storage capacity limitations of the energy storage devices are not considered. In the study, the effect of the adjustment of the charging threshold on the SC ESPP is explored, and the braking power satisfies the equation shown in (14).

$$P_b = P_{\mathrm{res}} + P_{\mathrm{ESS}} \tag{14}$$

In (14), P_{ESS} represents the charging power of the ESPP. When the on-board braking resistor is activated, the equation becomes shown in (15).

$$P_b = P_{\mathrm{res}} + P_{\mathrm{ESS}} + P_{\mathrm{br}} \tag{15}$$

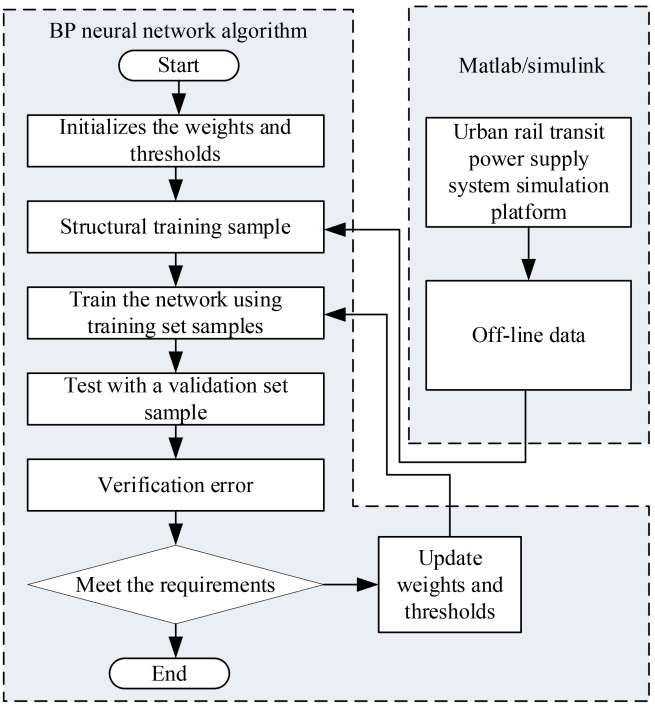

Figure 5. BP neural network specific training process.

In (15), P_{br} indicates that it is the power on the braking resistor. Adjusting the charging threshold can affect the charging power of the energy storage device, but too much energy is consumed on the braking resistor to affect the energy saving effect. Therefore, threshold adjustment is more critical in multi-train interaction systems. To study the impact of the threshold change of single ESS, a single energy storage device model is built as shown in Fig. 6 for a braking train and a traction train.

When the train braking resistance is not activated, the system power balance satisfies the relationship between P_t and P_{ss}, where P_t represents the traction power of the train, while P_{ss} represents the total output power of the three substations, and the specific balance relationship is shown in (16).

$$\begin{cases} P_b = P_t - P_{\mathrm{ss}} + P_{\mathrm{res}} + P_{\mathrm{ESS}} \\ P_{\mathrm{res}} = P_{r1} + P_{r2} + P_{r3} + P_{r4} \\ P_{\mathrm{ss}} = P_{\mathrm{ss1}} + P_{\mathrm{ss2}} + P_{\mathrm{ss3}} \end{cases} \tag{16}$$

In a multi-storage device system, in addition to RE absorption by the traction train, regenerative braking energy is also distributed to different storage devices. This multi-storage configuration provides more options for RE management and distribution than a single energy storage device system. To study this multiple ESS in more depth, a model is constructed as shown in Fig. 7, which contains three energy storage devices and a braking train.

When there is a braking train in the model, its distances from the three ESPPs are 1.9 km, 0.1 km, and 2.1 km. The train is braked with a power of 1.7 MW using 14 series and 12-parallel SC modules. The charging thresholds for ESS1 and ESS3 are 870 V while the main focus is on the variation of the charging thresholds for ESS2. When the braking resistor is not activated, the power of all three ESPPs satisfies a specific power balance condition as shown in (17).

$$\begin{cases} P_b = P_{\mathrm{ESS1}} + P_{\mathrm{ESS2}} + P_{\mathrm{ESS3}} + P_{\mathrm{res}} \\ P_{\mathrm{res}} = P_{r1} + P_{r2} + P_{r3} \end{cases} \tag{17}$$

In ESPP systems, whether single or multiple energy storage, properly adjusted charging thresholds can fully absorb braking energy and reduce line losses. When the energy storage device is likely to be full, an appropriate increase in the threshold can absorb excess braking energy with the surrounding traction train and other ESPPs. This helps to reduce or eliminate energy consumption on the braking resistor and achieve energy savings. Conventional control strategies have problems, such as the inability to coordinate the amount of energy stored in multiple energy storage devices and SCs. Therefore, a BPNN-based DT energy management strategy is proposed, as shown in Fig. 8. This strategy adds a BPNN module and a threshold calculation module to the traditional double-loop control. By detecting the position and power of the train in real time, this strategy can calculate the remaining RE of the SC ESPP and adjust the charging threshold accordingly.

The BPNN-based energy management strategy includes five core modules: the BPNN module, the threshold calculation module, the voltage outer loop module, the mode switching module, and the current inner loop module. Among them, the principles of the voltage outer loop module, mode switching module, and current inner loop module are the same as those of the traditional dual-loop energy management strategy. The threshold calculation module aims to adjust the charging threshold of the SC. When the SC is not full, the module maintains a lower charging threshold; when the SC is expected to be full, the charging threshold is appropriately increased. This adjustment helps to achieve energy saving effect, and the specific threshold calculation equation is shown in (18).

$$\begin{cases} U_{\mathrm{char}} = \begin{cases} U_0 + \Delta U_{\mathrm{char}}, E_p \le E_r \\ U_0 + \Delta U_{\mathrm{char}} + ka, E_p > E_r \end{cases} \\ E_r = \frac{1}{2}C(U_{\max}^2 - u_{\mathrm{sc}}^2) \\ a = (E_p - E_r)/\frac{1}{2}CU_{\max}^2 \\ U_{\mathrm{dis}} = U_0 - \Delta U_{\mathrm{dis}} \\ \Delta U_{\mathrm{char}}, \Delta U_{\mathrm{dis}} \ge 0 \\ k \ge 0 \end{cases} \tag{18}$$

In (18), U_{char} denotes the voltage outer loop charging threshold; u_{SC} denotes the SC module terminal voltage; U_{dis} denotes the discharging threshold; ΔU_{dis}, ΔU_{char}, and k are the three to-be-determined parameters; C and $U_{\max}$ denote the container and maximal point voltages of the SC storage device, respectively; and E_r denotes the residual energy storage capacity.

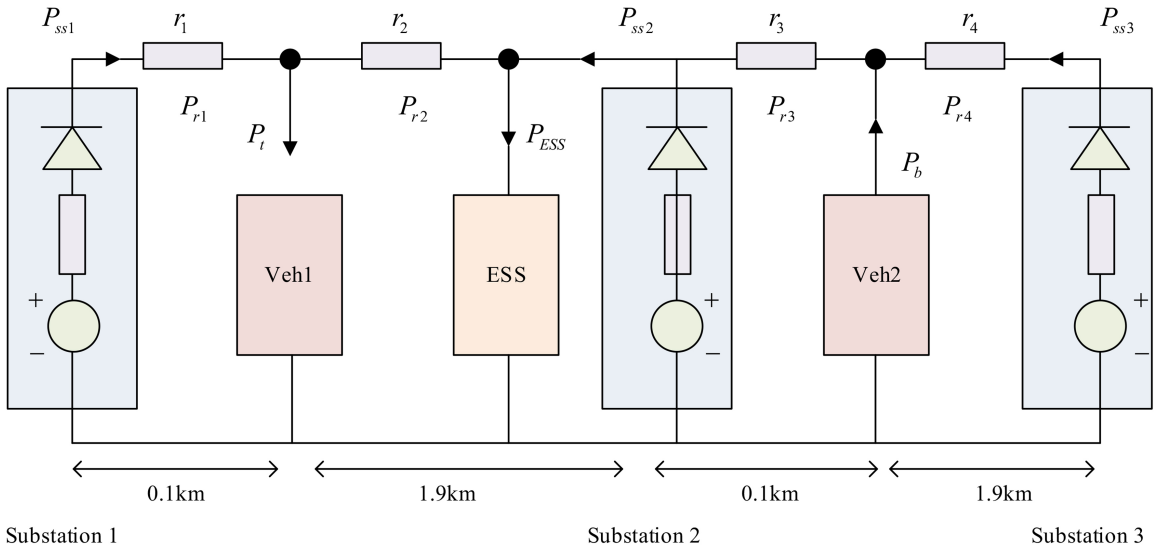

Figure 6. Single energy storage device system model.

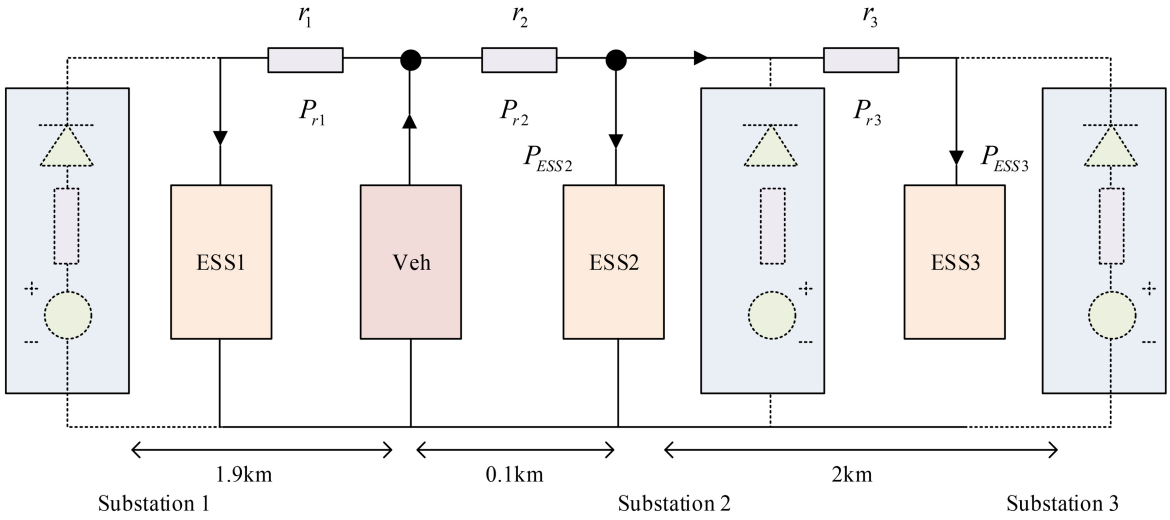

Figure 7. Multi-energy storage device model.

4. Simulation Analysis of Prediction and DT Management Strategies for RE

In this study, the well-trained prediction model is first validated through simulation to ensure its prediction accuracy under various headway intervals. Then, the study analyses the effect of the improvement strategy under single energy storage and multiple ESPP systems.

4.1 Simulation Analysis of Predictive Models

When building predictive models, it is key to model each ultracapacitor energy storage device individually. Here, three different BP neural network models are used. The charging threshold of all energy storage devices is set to 865 V, and 10,000 sets of input and output samples are obtained through traction power supply simulation platform. The data is divided into three parts: the training set, the validation set, and the test set. The study selected 70% (7,000 sets) of data as the training set, this part of the data is mainly used to determine the parameters of the network (such as weights and thresholds) and adjust these parameters according to the network error. Next, 15% (or 1,500 sets) of data are used as validation sets, which are used to monitor the network's generalisation ability and stop training if the generalisation performance is no longer improving. This step is to ensure that the generalisation ability of the neural network continues to increase. Finally, the remaining 15% (also 1,500) of the data is used as a test set, which is not used to improve network performance, but to evaluate the network that has been trained. The research experiment uses the neural network toolbox of MATLAB to build the network. Figure 9 shows the neural network. The toolbox uses the Levenberg-Marquardt algorithm (trainlm) for training. According to the above Settings, a single hidden layer BP neural network is selected, which has eight input nodes, one output node, and 104 hidden layer nodes. The maximum number of iterations of the network is set to 1,000.

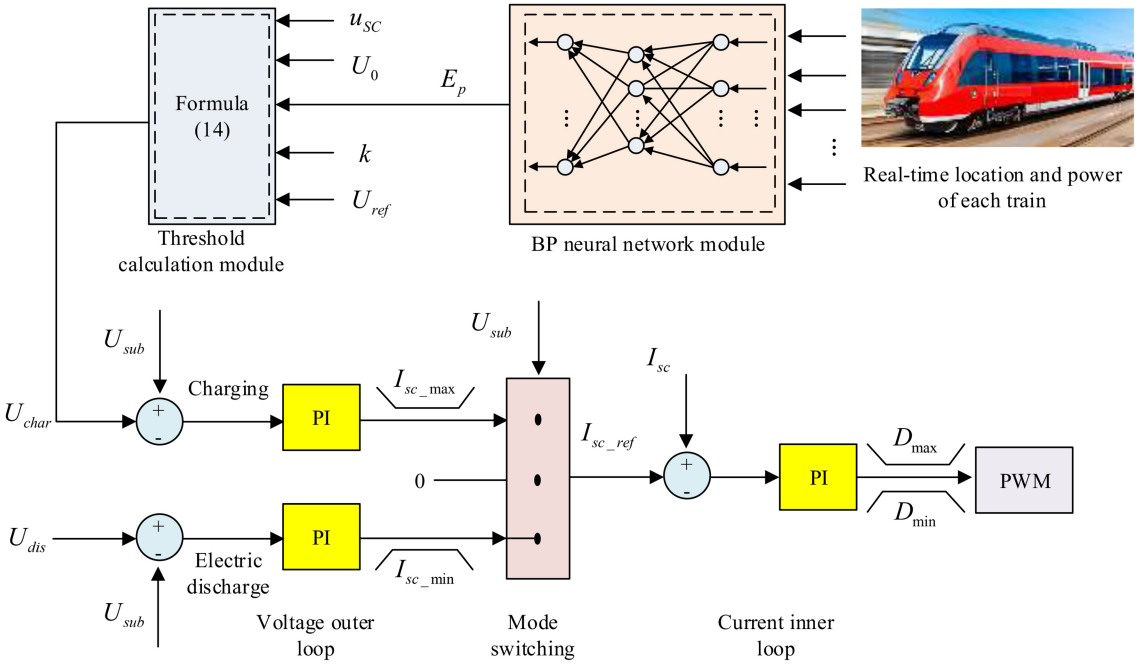

Figure 8. Dynamic threshold control block diagram of supercapacitor energy storage system.

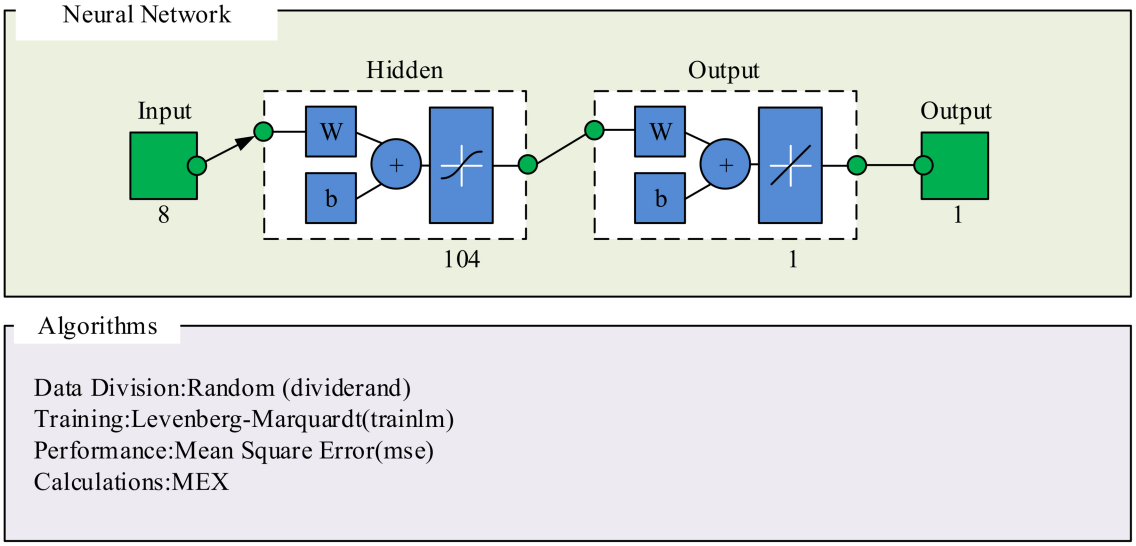

Figure 9. Neural network structure diagram.

In this research experiment, three prediction models of energy storage power stations were established, and ESS1 was taken as an example to show the prediction results, as shown in Fig. 10.

As demonstrated in Fig. 10(a), the best results are obtained at generation 272, where the mean square errors of the training, testing, and validation sets are 4.27×10^{-4}, 1.74×10^{-3}, and 2.95×10^{-3}, respectively. Iteration terminates at generation 278 of the validation set, as its generalisation ability is no longer enhanced. The error histogram in Fig. 10(b) shows that most of the sample errors are concentrated in a small range around 0.

According to Fig. 11, the goodness-of-fit R-values for each dataset are very close to 1. 0.9989 for the training set, 0.9928 for the confirmation set, 0.9958 for the test set, and 0.9974 for the overall samples, which shows that the BPNN has a high degree of accuracy in the prediction of RE. Further, Fig. 12(a) compares the actual RE with the predicted values for the three energy storage devices: the solid line represents the actual expected value and the dashed line is the predicted output of the network. These two lines largely overlap, further demonstrating the high accuracy of the model.

To compare the prediction results of the prediction models under multiple headway intervals, Fig. 12(b) demonstrates the prediction results for 400 s headway intervals, using the same neural network prediction module as for 300 s headway intervals. The expected and predicted values nearly overlap, proving that the BPNN model

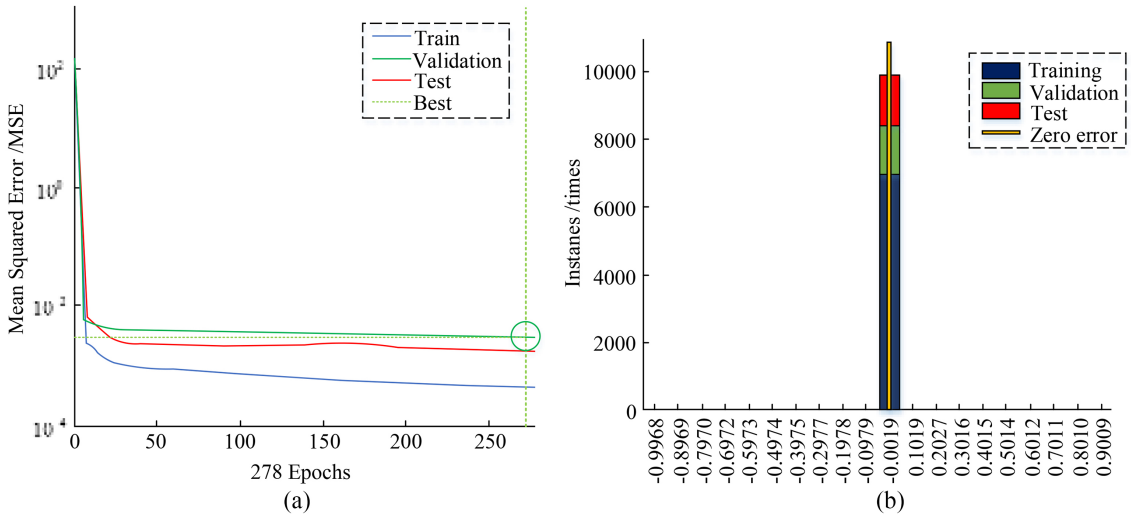

Figure 10. Training results: (a) iterative graph and (b) error histogram.

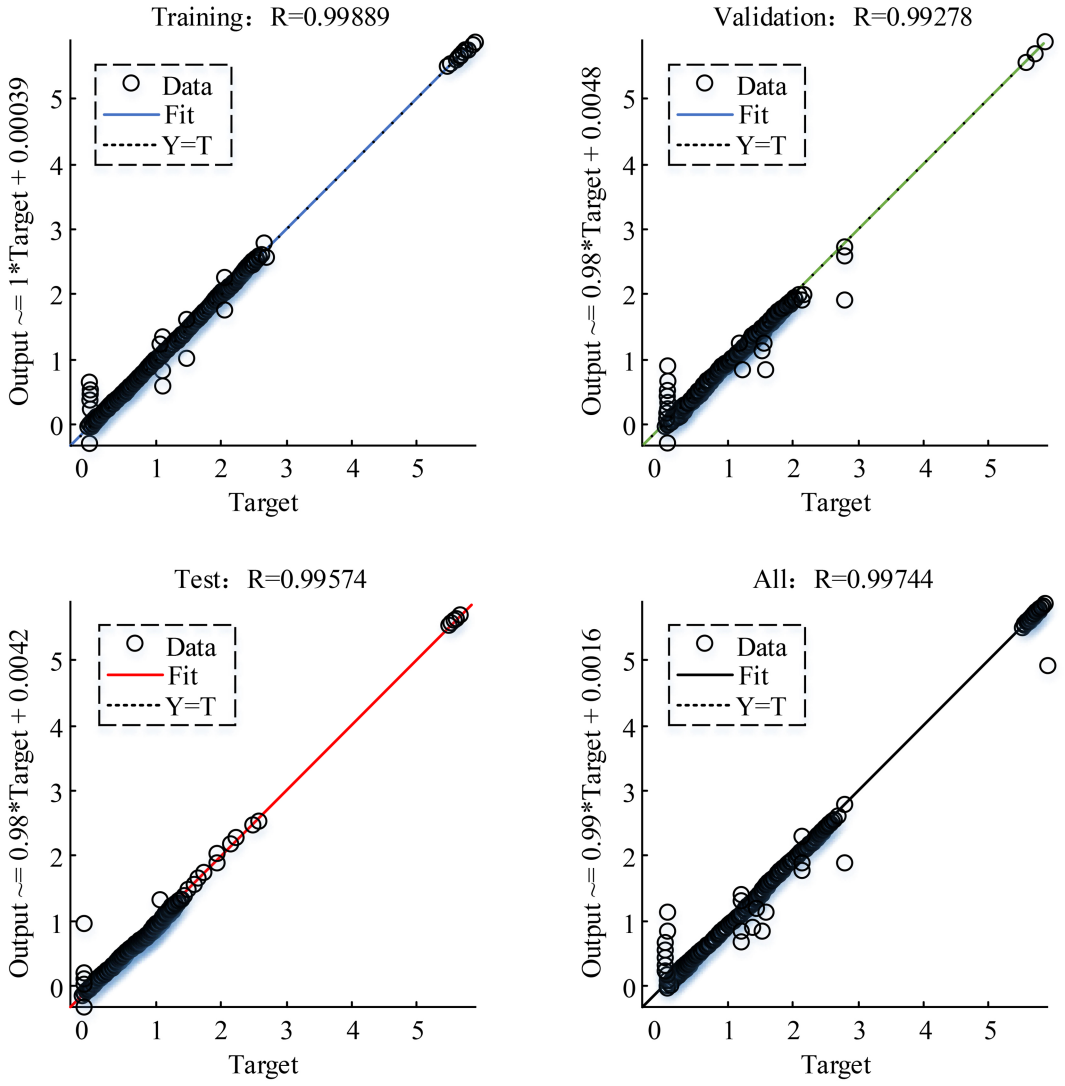

Figure 11. BP neural network model fitting diagram.

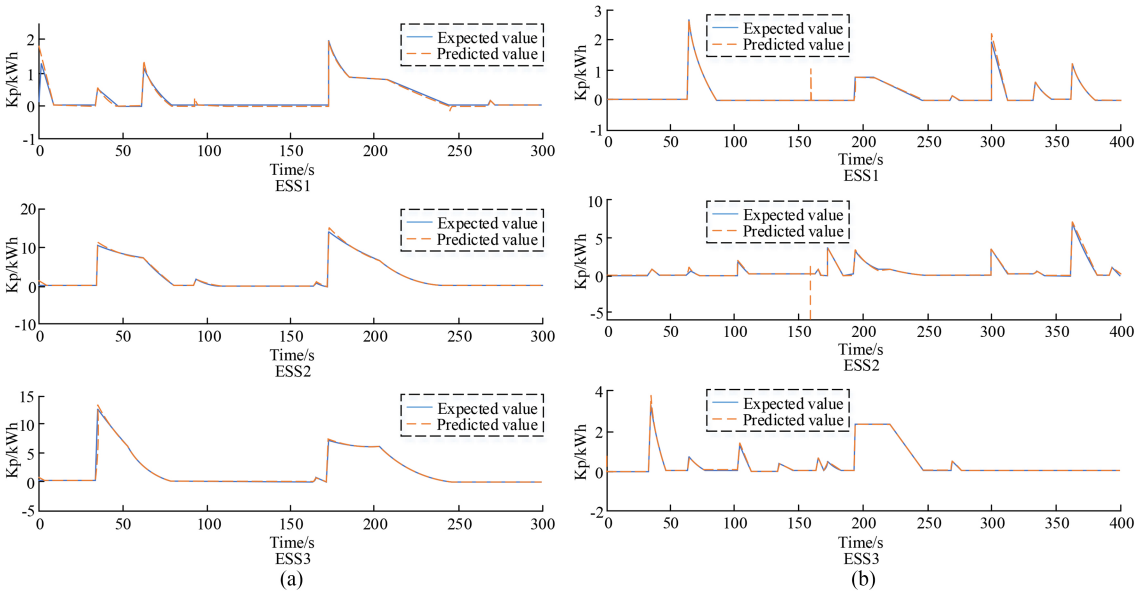

Figure 12. Prediction effect of 300 s and 400 s departure intervals: (a) prediction effect of 300 s departure interval and (b) prediction effect of 400 s departure interval.

shows excellent prediction ability under different departure intervals.

4.2 Comparison and Analysis of Improvement Strategies Under Single and Multiple ESPP Systems

The SC modules are connected in 14 series and 12 parallel. The peak power of the two braking vehicles is 1.5 MW, and the power of the traction vehicle is 1.8 MW. Figure 13(b) demonstrates the train power curves; Fig. 13(a) shows the simulation model, in which Train 1 is traction and Trains 2 and 3 are braking. The charging threshold of the conventional control strategy is set to 865 V and the parameters of the improved control strategy are $\Delta U_{\text{char}} = 5$, $\Delta U_{\text{dis}} = 0$, $k = 60$.

Figure 14(a) shows that the SC is filled and decommissioned first with the fixed threshold strategy, while the improved strategy extends it by about 5 s. Figure 14(b) demonstrates the change in braking resistor energy consumption, where the improved strategy extends its start-up time and reduces RE consumption. Figure 14(c) presents the SC charging threshold variation: at the beginning of charging, the charging threshold is increased due to the inability to fully absorb the RE, prompting the neighbouring tractor to absorb more energy. As the difference between E_p and E_r narrows, the threshold decreases. The improvement strategy adjusts the threshold according to the energy absorption by the ESS to assist the train in absorbing energy, delaying the braking resistor activation and mitigating the impact of energy storage on the train interaction energy.

Table 3 shows that the improved control strategy reduces the substation output energy by 0.753 kWh and the braking resistor energy consumption by 0.792 kWh compared to the conventional fixed-threshold strategy.

Table 3
Energy Output of Substation and Energy Consumption of Braking Resistance

Tactics	Output energy (kWh)	Resistance energy consumption (kWh)
Fixed threshold policy	2.77	1.21
Improved control strategy	2.01	0.42

This proves the superior energy saving effect of the improved strategy.

The SC modules are connected in 14 series and 12 parallel. The discharge threshold of both strategies is set to 860 V, which is flush with the no-load voltage of the substation, to ensure that the SC is completely discharged. The traditional strategy sets the charging threshold to 865 V, while the parameters of the DT strategy are $\Delta\Delta U_{\text{dis}} = 0$, $\Delta U_{\text{char}} = 5$, $k = 60$. The simulation model is shown in Fig. 15(a), where train 2 brakes at ESS2 from 7 s to 43 s, at which time trains 1 and 3 are in idling; train 1 starts braking at 62 s; and train 3 starts pulling at 79 s, when there are both pulling and braking trains on the line.

In Fig. 16 it is shown that the improved control strategy causes the charging threshold of ESS2 to be increased at the 7ths, resulting in ESS2 absorbing less energy and neighbouring ESPPs absorbing more. This is reflected in the SC voltage, suggesting that raising the threshold transfers braking energy to other ESPPs. ESS2 is fully charged and shut down at 34 s, resulting in an increase in the ESS1 voltage, but the improved strategy allows ESS2 to charge for a longer period of time, distributing the energy evenly. From 62 s, train 2 starts braking, and the BPNN module of ESS3 detects insufficient energy absorption,

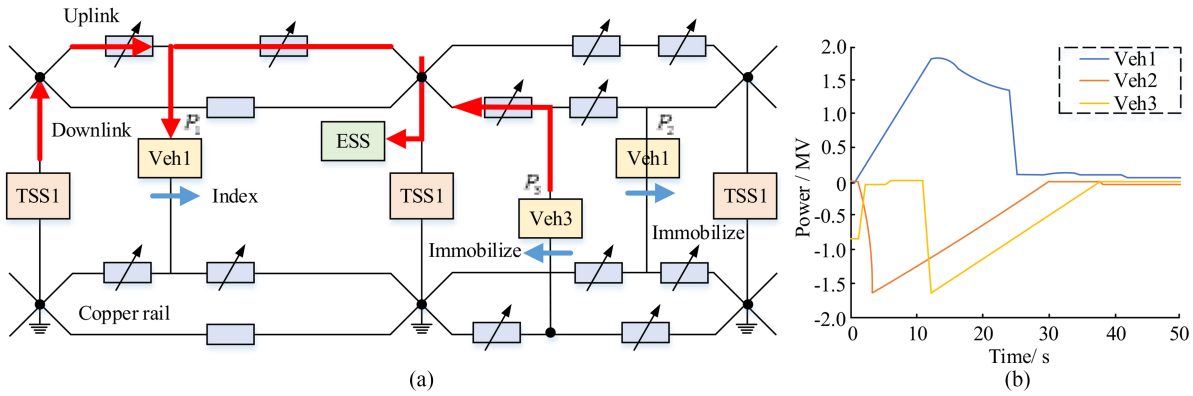

Figure 13. Simulation model and power curve diagram of the train: (a) simulation model diagram and (b) train power curve.

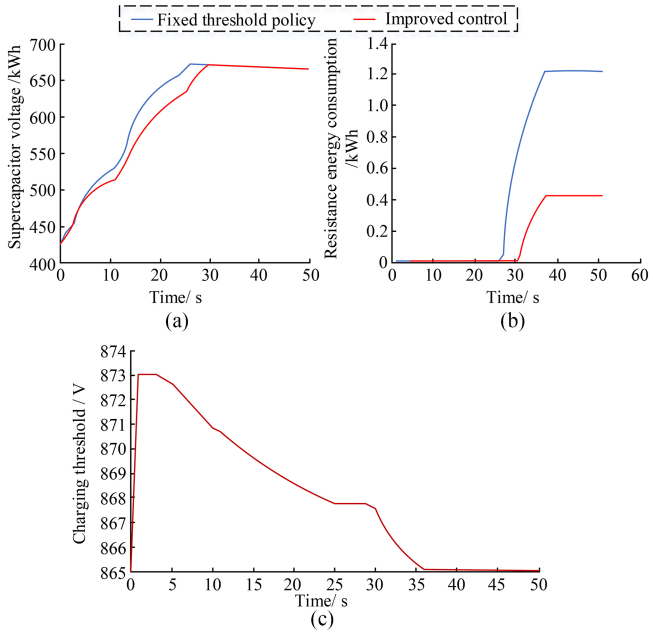

Figure 14. Supercapacitor voltage and threshold change diagram: (a) supercapacitor voltage; (b) resistance energy consumption; and (c) the supercapacitor threshold.

raises the charging threshold, and absorbs energy together with the nearby ESPP. However, since ESS2 is full, most of the RE flows to ESS1, increasing its charging power. The adjusted threshold leads to an increase in the charging time of ESS3 and a delay in braking resistor activation, which in turn saves energy. The peak value of the traction network voltage also decreases slightly.

According to the data in Table 4, the improved control strategy reduces the output energy of the substation by 0.2 kWh and the energy consumption of the braking resistor by 0.178 kWh compared to the conventional fixed-threshold energy management strategy. This proves that the improved strategy is effective in saving energy.

The study proposes an improved management strategy and compares it with the existing management strategy focusing on line loss consumption between two stations during the train start-up phase. Preliminary analyses show that the performance differences between the four different

Table 4
Energy Output of Substation and Energy Consumption of Braking Resistance

Tactics	Output energy (kWh)	Resistance energy consumption (kWh)
Fixed threshold policy	23.71	0.27
Improved control strategy	23.51	0.09

approaches during the start-up phase are not significant. To assess the line loss consumption in the start-up phase more clearly, the study narrowed down the analysis time to the interval of 0.215 s to 0.25 s, as shown in Fig. 17. During this period of time, the line loss consumption of the particle swarm optimisation algorithm management strategy increased from about 0.793 to about 0.802, while that of the locust optimisation algorithm management strategy increased from 0.79 to about 0.799. In contrast, the fixed threshold management strategy showed the worst performance in terms of line loss consumption. In contrast, the line loss consumption of the energy efficient management strategy proposed in the study increases from 0.762 to 0.789, showing lower linear consumption and better energy efficiency. It is worth noting that urban rail is not limited to two stations. In practical applications, the neural network algorithm proposed by the study performs better in reducing line loss consumption and enhancing energy saving compared to existing management strategies.

5. Conclusion

This study addresses issues related to the ground-based SC ESPP for URT systems, including the incapacity of the voltage–current double-loop control approach to manage numerous energy storage devices, the complexity of regulating the energy storage of SCs, and the significant impact of no-load voltage fluctuations. To tackle these problems, an upgraded energy management strategy that incorporates the characteristics of the ESPP and highlights multiple optimisation goals was introduced,

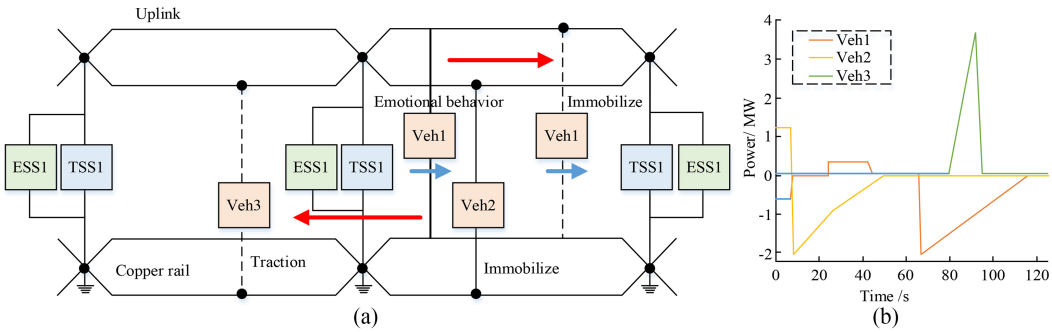

Figure 15. Simulation model and power curve diagram of the train: (a) simulation model diagram and (b) train power curve.

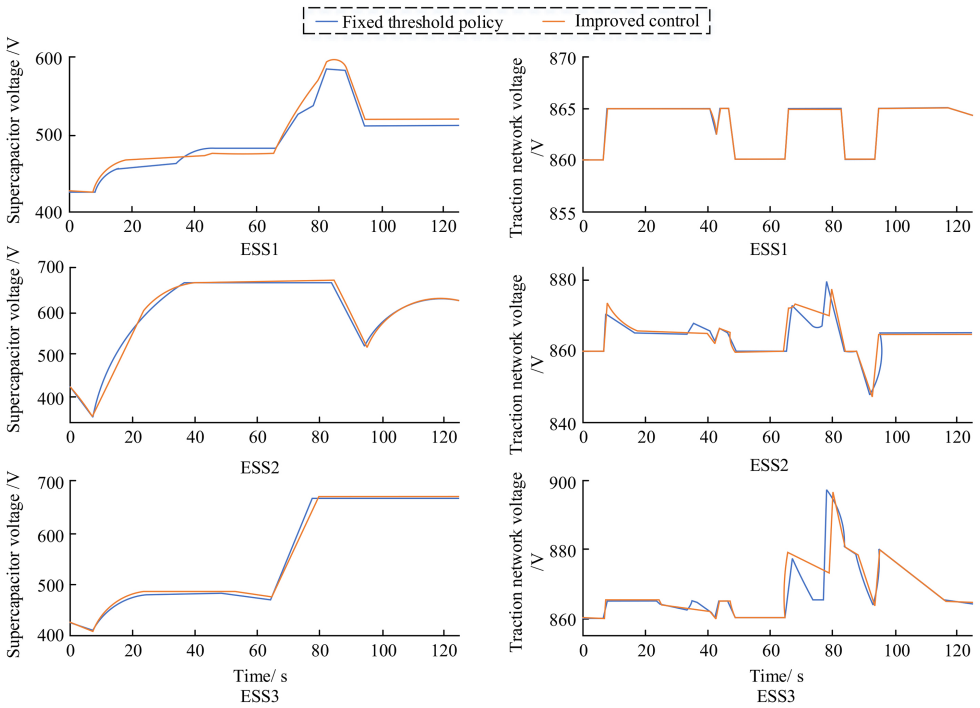

Figure 16. Comparison of the two strategies.

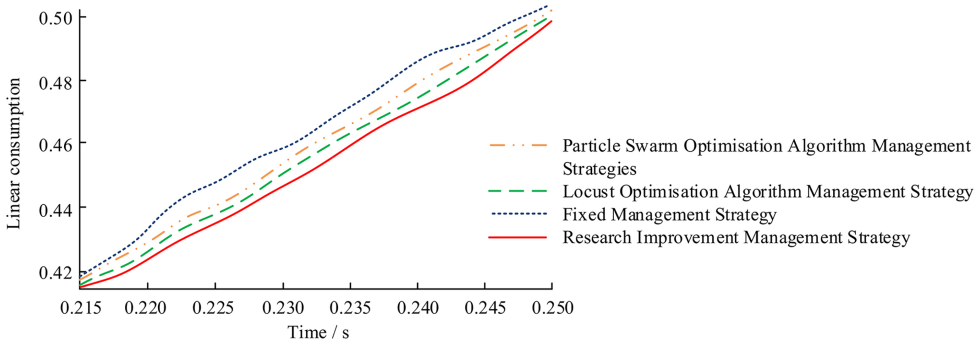

Figure 17. Comparison of consumption of different management policies.

relying on energy prediction by BPNNs. To test the effectiveness of this method, this study conducted a series of simulations and experiments. The findings indicated that the selected BPNN accurately predicted the RE. After 272 training cycles, the mean square error of the model was 4.27×10^{-4}, 1.74×10^{-3}, and 2.95×10^{-3} on the training, test and validation sets, respectively. This demonstrated its high prediction accuracy. This strategy enables accurate set up of the charging and discharging thresholds to maximise RE absorption by the SC in the ESPP, and increase the charging threshold when needed to foster energy interaction among multiple trains, ultimately

achieving a fair distribution of RE across diverse energy storage devices. Upon comparison with the traditional fixed-threshold strategy, the improved approach results in a reduction of 0.2 kWh in the output energy of the ESPP and 0.178 kWh in the energy consumption on the braking resistor, thus demonstrating its significant energy-saving effect. However, the study has certain limitations. For instance, the capacity configuration of the energy storage device was not extensively investigated and was only analysed based on specific configurations; the study was confined to a model with only three traction substations, and the overall line scenario was not investigated thoroughly, and the impact of threshold changes was analysed in a simplified model, while an in-depth analysis of the more complex system is yet to be carried out.

6. Discussion

The potential practical applications of this research are broad and far-reaching in the real world. First, in URT systems, the application of this research can significantly improve energy efficiency, especially in the face of traffic congestion and environmental problems in the process of urbanisation. By dynamically adjusting the charging demand of the energy storage power station, this strategy not only optimises the utilisation of energy but also promotes the collaborative work between multiple sets of ESSs, thereby improving the overall energy-saving effect and laying the foundation for green development in the transportation sector. Second, the strategy plays a key role in the management of complex power grid systems. It can effectively solve the complexity problem of DC traction power supply network and the actual power control challenge of ultracapacitors. In volatile renewable power supply systems, such as wind and solar, the application of this strategy helps to reduce the output energy and reduce the energy consumption of the brake resistance. In addition, by precisely adjusting the charge and discharge threshold, the strategy can also realise the balanced distribution of renewable energy among energy storage devices and promote the energy interaction between multiple trains, thus improving the stability and energy utilisation of the power grid. Finally, the improved energy management strategy based on BP neural networks proposed in the study, while currently computationally intensive, provides a basis for the development of more efficient machine learning frameworks, especially in prioritising the protection of large cyber-physical systems. In future studies, based on the current results, we can further explore the capacity configuration of energy storage devices, expand the scope of research to cover the whole line of more traction substations, and conduct in-depth analysis of the impact of threshold changes on more complex systems. These explorations not only help improve the effectiveness of existing strategies but also provide more comprehensive solutions for modern urban transportation systems and large-scale grid management.

7. Funding

The research is supported by: Yunnan Power Grid Co. Ltd. Technology project plan, Project No: YNKJXM20230074.

References

[1] A.Z. Arsad, M.A. Hannan, A.Q. Al-Shetwi, M. Mansur, K.M. Muttaqi, Y.Z. Dong, and F. Blaabjerg, Hydrogen energy storage integrated hybrid renewable energy systems: A review analysis for future research directions, *International Journal of Hydrogen Energy, 47*(39), 2022, 17285–17312.

[2] M. Asker, D. Akal, and M.A. Ezan, Performance assessment of a phase change charging mode in a vertical thermal energy storage system, *International Journal of Energy Research, 46*(6), 2022, 7610–7625.

[3] Z. Yu, W. Feng, X. Sun, Z. Gu, and C. Wen, 3D electromagnetic behaviours and discharge characteristics of superconducting flywheel energy storage system with radial-type high-temperature bearing, *IET Electric Power Applications, 14*(10), 2020, 1865–1872.

[4] Y. Liu, Z. Yang, X. Wu, D. Sha, F. Lin, and X. Fang, An adaptive energy management strategy of stationary hybrid energy storage system, *IEEE Transactions on Transportation Electrification, 8*(2), 2022, 2261–2272.

[5] K.M. So, G.S. Hong, and W.F. Lu, An improved speed-dependent battery/ultracapacitor hybrid energy storage system management strategy for electric vehicles, *Proceedings of the Institution of Mechanical Engineers, Part D: Journal of Automobile Engineering, 235*(14), 2021, 3459–3473.

[6] S. Nimrah and S. Saifullah, Context-free word importance scores for attacking neural networks, *Journal of Computational and Cognitive Engineering, 1*(4), 2022, 187–192.

[7] F. Keynia and G. Memarzadeh, A new financial loss/gain wind power forecasting method based on deep machine learning algorithm by using energy storage system, *IET Generation, Transmission & Distribution, 16*(5), 2022, 851–868.

[8] T.E. Balaji, H.T. Das, and M. Thandavarayan, Recent trends in bimetallic oxides and their composites as electrode materials for supercapacitor applications, *Chem Electro Chem, 10*(8), 2021, 1723–1746.

[9] S.U. Nisa and U.D. Mufti, Constrained discrete mode control of supercapacitor energy storage system for improved AGC of a multi-area power system with effects of wind power, *International Journal of Power Electronics: IJPElec, 14*(3), 2021, 386–403.

[10] V. Mali and B. Tripathi, Thermal stability of supercapacitor for hybrid energy storage system in lightweight electric vehicles: Simulation and experiments, *Journal of Modern Power Systems and Clean Energy, 10*(1), 2022, 170–178.

[11] H. Shadabi and I. Kamwa, Enabling hybrid energy storage systems in VSC-based MTDC grids for decentralized fast frequency response control in low-inertia AC/DC systems, *IET Generation, Transmission & Distribution, 16*(5), 2022, 897–911.

[12] M.E.C. Bento, Physics-guided neural network for load margin assessment of power systems, *IEEE Transactions on Power Systems*, *39*(1), 2024, 564–575.

[13] W. Liao, S. Wang, B. Bak-Jensen, J.R. Pillai, Z. Yang, and K. Liu, Ultra-short-term interval prediction of wind power based on graph neural network and improved bootstrap technique, *Journal of Modern Power Systems and Clean Energy*, *11*(4), 2023, 1100–1114.

[14] M. Kiannejad, M.R. Salehizadeh, and M. Oloomi-Buygi, Two-stage ANN-based bidding strategy for a load aggregator using decentralized equivalent rival concept, *IET Generation, Transmission & Distribution, 15*(1), 2021, 56–70.

[15] Y. Li, J. Cao, Y. Xu, L. Zhu, and Z.Y. Dong, Deep learning based on Transformer architecture for power system short-term voltage stability assessment with class imbalance, *Renewable and Sustainable Energy Reviews, 189*, 2024, 113913.

[16] M. Mohammadamin, Y. Weng, and Y. Lai, Defending smart electrical power grids against cyberattacks with deep Q-learning, *P R X Energy, 1*, 2022, 033005.

[17] A. Mosavi, M. Salimi, S. Faizollahzadeh Ardabili, T. Rabczuk, S. Shamshirband, and A.R. Varkonyi-Koczy, State of the art of machine learning models in energy systems, a systematic review, *Energies, 12*(7), 2019, 1301.
[18] M. Moradi, Y. Weng, J. Dirkman, and Y.C. Lai, Preferential cyber defense for power grids, *PRX Energy, 2*(4), 2023, 043007.
[19] Z. Chen, Research on internet security situation awareness prediction technology based on improved RBF neural network algorithm, *Journal of Computational and Cognitive Engineering, 1*(3), 2022, 103–108.
[20] A.R. Saxena and A. Kulshreshtha, A fourth-order bidirectional DC-DC converter for interfacing battery in a solar - photovoltaic-fed low-voltage residential DC nano-grid: Design and analysis, *International Journal of Circuit Theory and Applications, 49*(7), 2021, 1932–1958.
[21] V.M. Praveen, R. Vigneshkumar, and N. Karthikeyan, Heat transfer enhancement of air-concrete thermal energy storage system – CFD simulation and experimental validation under transient condition, *Proceedings of the Institution of Mechanical Engineers, Part E: Journal of Process Mechanical Engineering, 235*(5), 2021, 1304–1314.
[22] S. Debnath, Fuzzy quadripartitioned neutrosophic soft matrix theory and its decision-making approach, *Journal of Computational and Cognitive Engineering, 1*(2), 2022, 88–93.

Biographies

Xiuquan Li received the bachelor's degree in electrical engineering and automation from Shenyang University of Engineering in 2009. He currently works in the field of incident power operation with Yunnan Qujing Power Supply Bureau of China Southern Power Grid. He has been invited multiple times as the Deputy Leader of the Digital Transformation Acceptance Work Group for Yunnan Power Grid Company's substation operation to carry out the construction acceptance work of the full function inspection and maintenance center. His areas of interest include RPA robot applications, remote operation and maintenance of equipment videos, and standardized construction of teams.

Mingwan Zhuang received the bachelor's degree in power systems and automation from Kunming University of Technology in 2002. He is currently a Level 3 Leading Skill Expert and a Specialist in substation operation with Qujing Power Supply Bureau, Yunnan Power Grid Company. Has won five awards in various categories in the power industry of Yunnan Province. His main interest is in innovative research related to digital transformation in the power industry.

Weirong Yang is a Senior Engineer, a Substation Technical Expert, a Technical Supervision and condition monitoring of Yunnan Power Supply Bureau Co., Ltd. He has been working in power system for 27 years. His areas of interest include RPA robot applications, remote operation and maintenance of equipment videos, and standardized construction of teams.

Xiaohong Zhu received the master's degree in control theory and control engineering from Chongqing University in 2006. He currently works with Qujing Power Supply Bureau, Yunnan Power Grid Co., Ltd., engaged in the operation and maintenance of power system relay protection. His areas of interest include RPA robot applications, remote operation and maintenance of equipment videos, and standardized construction of teams.

Qiyuexin Wang was born in July 2001 in Kunming, Yunnan, China. She graduated from Huaqiao University. She is currently pursuing the graduation degree with Kunming University of Science and Technology. Her research direction is new energy materials.